LARGE-EDDY SIMULATION OF A JET IMPINGING ON A MOVING SURFACE

Himadri Chattopadhyay
Central Mechanical Engg. Research Instt.,
Durgapur – 713209, India

Gautam Biswas
Dept. of Mechanical Engg., Indian Instt. of Technology,
Kanpur- 208016, India

Nimai K. Mitra
Institut für Thermo –und Fluiddynamik,
Ruhr Universität Bochum,
44780 Bochum, Germany

ABSTRACT

Flow and heat transfer due to a slot jet impinging on a moving surface has been investigated using a dynamic subgrid scale model of Large-eddy simulation. The velocity of the impingement surface has been varied up to two times the velocity of jet at the nozzle exit. A fractional time-step method has been use to solve the filtered Navier-Stokes equation. Turbulence quantities such as kinetic energy of turbulence, production rate of turbulence and Reynolds stresses, are calculated from the flow field data. Nusselt number distribution over the impingement plate at different surface velocity is presented.

INTRODUCTION

Heating, cooling or drying of a moving surface by impinging jets is a common industrial practice. Though jet impingement is a subject of considerable interest to researchers, relatively fewer studies have reported the effect of surface motion on the jet impingement transfer processes.

Earlier studies (Chen et al 1994, Zumbrunnen et al., 1991, 1992) have shown that the moving impingement surface strongly influences the flow field and thus heat transfer. However the lack of literature forces the industry to rely solely on operating experiences and rule of thumb which may not be desirable in processes where quality is determined by the amount and uniformity of heat transfer, e.g., metals manufacturing. It may also be necessary to include the effect of horizontal motion in case of VSTOL aircrafts.

In the numerical study of Huang et al.(1984), a cross flow of fluid in the direction of surface motion was incorporated to simulate flow from the adjacent jets and to tackle fluid entrainment on the moving surface. They reported that at higher plate speeds, Nusselt number was smaller at the locations where the surface motion opposed the dividing jet flow, and higher where the surface motion and dividing jet flow are in the same direction.

Chen et al.(1994) developed a numerical model to determine convective heat transfer distributions in the laminar range for an array of submerged planar jets impinging on a uniform heat flux or constant temperature moving surface where the surface motion is directed perpendicular to jet planes. With increasing plate speed flow separation near the flow-merging plane did not occur, heat transfer distributions became more uniform but the total heat transfer reduced.

The flow fields of impinging jets are complex and may contain laminar, transitional and turbulent zones. A direct numerical simulation (DNS) is undoubtedly the best approach to reveal the details of such complex flows. However, in DNS the number of grid points needed is of the order of $Re^{9/4}$ so that all scales of motion are resolved. Large eddy simulation (LES) is a technique intermediate between the direct simulation of turbulent flows and the solution of the Reynolds-average equations through closure approximations. Since the small scales are more homogeneous and universal and less affected by the boundary conditions than the large eddies, the modelling effort is less.

Recently Cziesla et al. (1997,1998) have reported the flow structure of an impinging slot jet using a dynamic subgrid model of LES. Turbulent quantities such as kinetic energy, production rate and its components were calculated and the stress budget captured locally negative turbulence production rate successfully.

The purpose of present work is to perform LES of the flow field of axial jets emanating from a rectangular slot nozzle and impinging on a moving surface. The movement of the plate is perpendicular to the jet motion at the exit of the nozzle. While the Reynolds number for the present study was 5800, the surface velocity of the impingement surface was varied up to two times the jet velocity at nozzle exit. It was expected that the results of the present investigation will elucidate the flow structure and form a data base of

turbulence variables for such a configuration. As such generating such data from experimentation is quite demanding in terms of planning, facilities and cost of experimentation. A CFD tool can thus become quite useful in order to obtain a first estimate of the flow structure.

The computational domain has been depicted in Fig. 1. It consists of a semi-enclosed rectangular slot jet of width B and length L_x. Periodicity of the flowfield has been assumed in y-direction. Convective boundary condition has been employed at x= 0 and 10.

BASIC EQUATIONS

The method of LES involves the application of a filter operation to the three-dimensional, time-dependent Navier-Stokes equations. The larger scales are solved directly, whereas the subgrid scales have to be modelled. Equations (1), (2) and (3) are the conservative, nondimensional and incompressible continuity, momentum and energy equations, written for the large scales which are denoted by an overbar

$$\frac{\partial \bar{u}_i}{\partial x_i} = 0 \qquad (1)$$

$$\frac{\partial \bar{u}_i}{\partial t} + \frac{\partial \bar{u}_i \bar{u}_j}{\partial x_j} = -\frac{\partial \bar{p}}{\partial x_i} + \frac{1}{\mathrm{Re}} \frac{\partial^2 \bar{u}_i}{\partial x_j^2} - \frac{\partial \tau_{ij}}{\partial x_j} \qquad (2)$$

$$\frac{\partial \bar{T}}{\partial t} + \frac{\partial \bar{u}_j \bar{T}}{\partial x_j} = \frac{1}{\mathrm{Re\,Pr}} \frac{\partial^2 \bar{T}}{\partial x_j^2} - \frac{\partial q}{\partial x_j} \qquad (3)$$

with

$$\tau_{ij} = \overline{u_i u_j} - \overline{u_i} \overline{u_j}, \qquad (4)$$

and

$$q = -\overline{u_{j''} T} = \frac{2}{\mathrm{Pr}_t} \overline{\nu_T} \frac{\partial \bar{T}}{\partial x_j} \qquad (5)$$

where ν_T is eddy viscosity. In Eq. (2) and (3) the Reynolds number Re_{2B} is based on the nozzle inlet velocity u_{in} and the hydraulic diameter of the geometry 2B. Pr is the Prandtl number which is defined as Pr=ν/a with the kinematic viscosity ν and the thermal diffusivity a. The turbulent Prandtl number Pr_t was assumed unity. Equation (3) yields a temperature field which is used for the calculation of Nusselt numbers.

Subgrid Closure Model

The term τ_{ij} in equation (4) is the contribution of small scales to the large scale transport equation, which has to be modelled.

The most commonly used subgrid scale model is based on the gradient transport hypothesis which correlates τ_{ij} to the large scale strain-rate tensor

$$\tau_{ij} = -2\nu_T \bar{S}_{ij} + \frac{\delta_{ij}}{3} \tau_{kk} \qquad (6)$$

where, δ_{ij} is Kronecker delta $\tau_{kk} = \overline{u_k' u_k'}$ and $\bar{S}_{ij}$ is given by

$$\bar{S}_{ij} = \frac{1}{2}\left(\frac{\partial \bar{u}_i}{\partial x_j} + \frac{\partial \bar{u}_j}{\partial xi} \right) \qquad (7)$$

Lilly (1992) proposed an eddy viscosity proportional to local large scale deformation

$$\nu_T = (C_S \Delta)^2 |\bar{S}| \qquad (8)$$

Here C_S is a constant, $\bar{\Delta}$ is the grid filte scale and $|\bar{S}| = (2\bar{S}_{ij}\bar{S}_{ij})^{1/2}$. Invoking (8) in (6) yields

$$\tau_{ij} - \frac{\delta_{ij}}{3}\tau_{kk} = -2C\Delta^2 |\bar{S}| \bar{S}_{ij} = -2C\beta_{ij} \qquad (9)$$

The quantity C is the Smargorinsky coefficient (basically this is square of the original quantity) depends on the type of flow under consideration. Lilly(1992) suggested a method to calculate C for each time step and grid point dynamically from the flow field data. In addition to the grid filter which signifies the resolved and subgrid scales, a test filter is introduced for computation of C. The width of the test filter is larger than the grid filter width.

Our computations were carried out using the model suggested by Piomelli and Liu (1995). Ill-conditioning of C leads to numerical irregularities which may be stabilized by a local averaging procedure in at least in one homogenous direction. Zang et al. (1996) proposed a local averaging over adjacent grid cells for the computation of recirculating flow. Since the present problem is also a complex three-dimensional flow with no homogeneous space direction, it was decided to implement this method.

METHOD OF SOLUTION

The basic equations have been solved by a fractional step finite difference technique due to Kim and Moin (1985). For the convective terms Adams-Bashforth scheme is used to get second order time discretization. A Crank-Nicholson scheme is used to discretize the diffusive terms. The program uses a co-located grid arrangement for discretization.

RESULTS AND DISCUSSIONS

Computations have been performed with a grid of 152 x 22 x 79 = 264176 cells. The size of Δx is 0.05 between x=-0.5 and +0.5. Outside this region, Δx has been increased continuously by 1 percent. In the y direction, a uniform grid of Δy=0.1 has been used. In the z direction, Δz=0.00469 has been used on the impingement plate and then Δz has been increased in the normal direction continuously by a factor of 1.14. For time-averaging, 200 instantaneous fields over 40000 time steps have been used. The computations have been performed on an IBM RISC 6000 - 58 H dedicated workstation. Due to lack of data for jet impingement flow on moving surface, code validation was performed for a stationery impingement plate [see Cziesla et al., 1997].

The non-dimensional turbulent kinetic energy k is defined as

$$k = \frac{1}{2} < u_i'' u_i'' > \qquad (10)$$

The turbulent kinetic energy has been averaged over the width and the contour lines of constant turbulent kinetic energy for different values of surface velocity over the x-z plane have been shown in Fig. 2. The maximum value of k is found to be 0.046,

0.049, 0.050 and 0.106 for corresponding surface velocity of 0.1, 0.5, 1.0 and 2.0 respectively. An analysis of field data for kinetic energy shows that while at u_s = 0.1 and 0.5, the location of maximum k is at a distance of 0.078 from the impingement surface at x = 1.3 and 1.46 respectively (i.e. at the left side of the computational domain), the location of peak kinetic energy shifts upward, i.e. at a distance of 0.558 from the impingement surface at x = 4.7 (almost below the impingement point) for u_s = 1.0. For u_s = 2.0, the location of peak k is at a distance of 0.08 from the impingement surface at x = 3.4, i.e. at the left side of the impingement point.

The turbulence production rate P_{ij} is given by

$$P_{ij} = -\langle u_i'' u_j'' \rangle \frac{\partial \langle u_i \rangle}{\partial x_j} \qquad (11)$$

Figure 4 shows the contour-lines related to production rate of turbulence, P_{ij} for u_s= 0.1 and 1.0. An analysis of field data for P_{ij} revealed values of maximum P_{ij} increases and the location of maximum P moves upward up to u_s = 1.0, and then the value of P drops considerably while the location shifts close to impingement surface at z= 0.078. The maximum values of P are .0043, .0071, .0109 and .0073 for u_s = 0.1, 0.5, 1.0 and 2.0 respectively. Distribution of P_{ij} at different surface velocities are shown in Fig. 4

Four components of Pij can be expressed as :

$$P_{11} = -\langle u''u'' \rangle \frac{\partial \langle u \rangle}{\partial x}$$

$$P_{13} = -\langle u''w'' \rangle \frac{\partial \langle u \rangle}{\partial z}$$

$$P_{31} = -\langle u''w'' \rangle \frac{\partial \langle w \rangle}{\partial x}$$

$$P_{33} = -\langle w''w'' \rangle \frac{\partial \langle w \rangle}{\partial z}$$

For a stationery impingement surface it was reported that in the stagnation region, the production rate is dominate by P_{11} and away from the stagnation region P_{13} becomes dominant (Cziesla, 1998). Now for the case of impingement surface in motion, a detailed analysis of all the components of turbulent production revealed that P_{33} is dominant term for u_s = 0.1, 0.5 and 1.0. At u_s = 2.0, major contribution to turbulent production comes from P_{13} and P_{11}. While in Fig. 5, distributions of P_{33} at us = 0.5 and 1.0 are shown, Fig. 6 and 7 show the distribution of P_{11} and P_{13} for u_s =2.0. The profiles of P33 distribution up to u_s=1.0 are similar to the distribution of P_{ij}. It is also evident from figures 4-7 that the turbulence production is confined within a thin zone near the impingement plate.

At u_s= 0.1, it was found that at the location of maximum P_{ij} magnitude of $\langle w''^2 \rangle$ is almost twice the value of $\langle u''^2 \rangle$, while the value of $\langle u''w'' \rangle$ is only about -0.001 At u_s= 0.5, at the location of maximum p production values of $\langle w''^2 \rangle$ is 0.05 while that of $\langle u''^2 \rangle$ is 0.015. The value of $\langle u''w'' \rangle$ is also too small (about 0.001) to influence p_{13} or p_{31}. At u_s = 1.0, at x = 4.5 and 5.5 the value of $\langle w''^2 \rangle$ is almost seven times that of $\langle u''^2 \rangle$ (Fig.s 8 and 9). Thus at us = 0.1, 0.5 and 1.0 major contributions come from P_{33}. However at u_s = 1.0, contribution from p_{13} becomes significant at x = 4.5 (left of the impingement point) as the occurrence of highest value of $\langle u''w'' \rangle$ coincides with that of high $\partial\langle u \rangle/\partial z$.

At u_s = 2.0, maximum value of $\langle u''^2 \rangle$ (Fig. 10) is much greater than that of $\langle w''^2 \rangle$. From Fig.11 we also observe that the value of u'w' is as large as -0.003 near the impingement surface and higher values are discerned only at the left side of the impingement point. Thus P_{11} and P_{13} are the major contributors to turbulence production term.

From the solutions of the energy equation, the global and local Nusselt numbers have been calculated. The values of time-mean global Nu are 34.09,38.58,41.25 and 39.22 for u_s = 0.1, 0.5, 1.0 and 2.0 respectively. The corresponding values for fixed surface is 33.47. Thus Nu increases with increasing surface motion and then decrease (see Subba Raju et al. 1977). From Fig. 12 it can be seen that the distribution pattern tends to be more uniform as the surface velocity increases.

Acknowledgment: German Academic Exchange Service (DAAD) for a research fellowship to HC.

REFERENCES

Chen, J., Wang, T., Zumbrunnen, D.A.,1994, "Numerical Analysis of Covective Heat Transfer From a Moving Plate Cooled by an Array of Submerged Planar Jets", *Num. Heat Transfer, Part A*, Vol. 26, pp. 141-160.

Cziesla, T., Tandogan, E. and N.K. Mitra, 1997, "Large Eddy Simulation from Impinging Slot Jets", *Num. Heat Transfer , Part A*, Vol. 32, pp. 1-17.

Cziesla, T., 1998, "Grobstruktursimulation der Strrömungs – und Temperatur felder von Prallstrahlen aus Sclitzdüsen", Disseratation, Ruhr Universität Bochum, , Reihe 19, Nr. 108, VDI Verlag, Düsseldorf

Huang, P.G., Mujumdar, A.S. and Douglas, W.J.M., 1984,"Numerical Prediction of Fluid Flow and Heat Transfer under a Turbulent Impinging Slot Jet with Surface Motion and Crossflow", ASME paper 84-WA/HT-33.

Kim, J., Moin, P., 1985, "Application of a Fractional-Step Method to Incompressible Navier-Stokes Equations", J. Comp. Physics, Vol. 59, pp. 308-323.

Lilly, D.K.,1992, "A Proposed Modification of the Germano Subgrid-Scale Closure Method", *Phys. Fluids A*, Vol. 4, No. 3, pp. 633-635.

Piomelli, U., and Liu, J., 1995, "Large-eddy simulation of rotating channel flows using a localized dynamic model", Phys. Fluids, Vol. 7, 839-848.

Subba Raju, K., Schlunder, E.U., 1977, "Heat Transfer between an Impinging Jet and a Continiously Moving Surface", *Wärme-Stoffübertr.*, Vol. 10, pp. 131- 136.

Zang, Y., Street, R.L., Koseff, J.R., 1993, "A Dynamic Subgrid-Scale Model and its Application to Turbulent Recirculating Flows", *Phys. Fluids A*, Vol. 5, No. 12, pp. 3186-3196.

Zumbrunnen, D.A., 1991, "Convective Heat and Mass Transfer in the Stagnation Region of a Laminar Planar Jet Impinging on a Moving Surface", *AME J. Heat Transfer*, Vol. 113, pp. 563-570.

Zumbrunnen, D.A., Incropera, F.P. and Viskanta, R., 1992, "A Laminar Boundary Layer Model of Heat Transfer due to a Nonuniform Planar Jet Impinging on a Moving Plate", *Wärme-Stoffübertr.* , Vol. 27, pp. 311- 319.

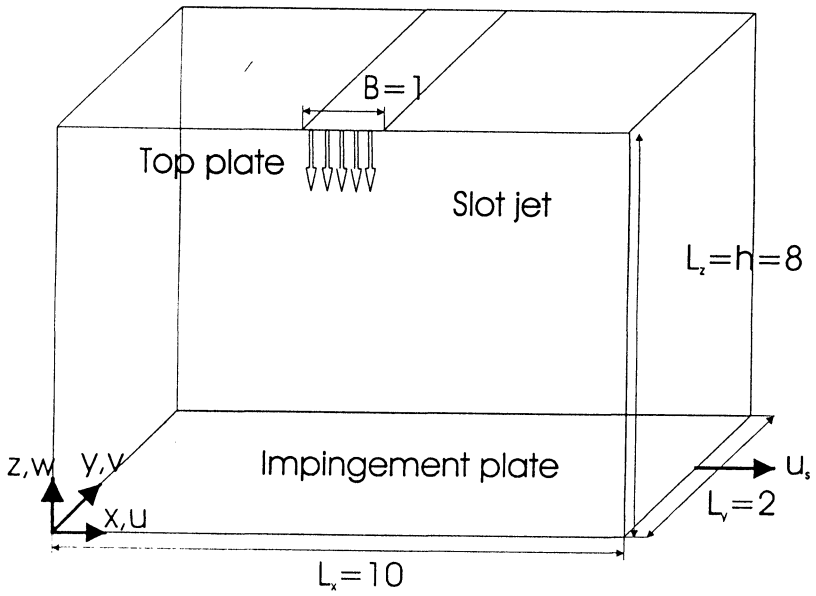

Fig. 1 Computational domain

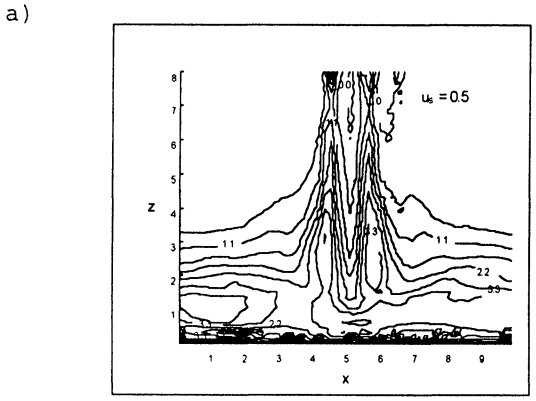

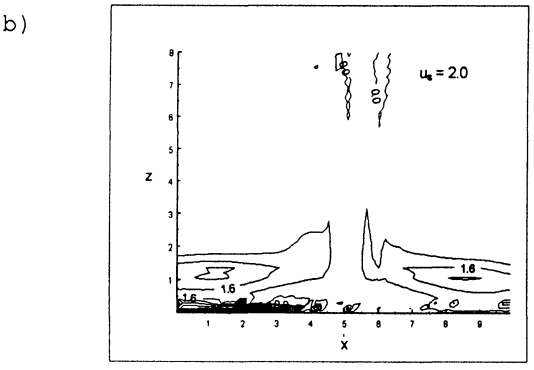

Fig. 2 Contours of turbulent kinetic energy (K*100)

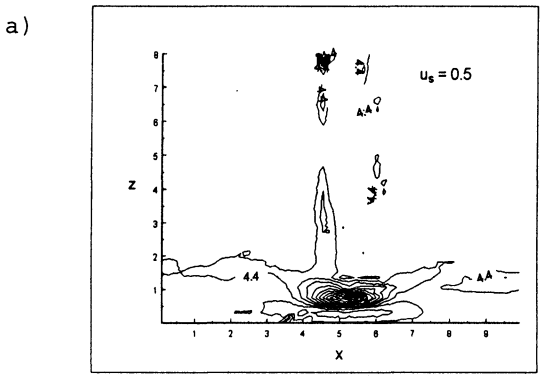

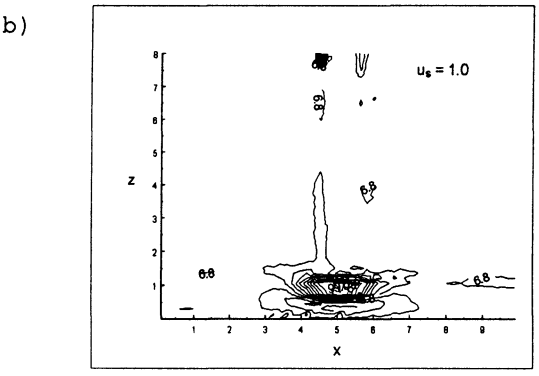

Fig. 3 Contours of turbulence production rate ($P*10^4$)

a)

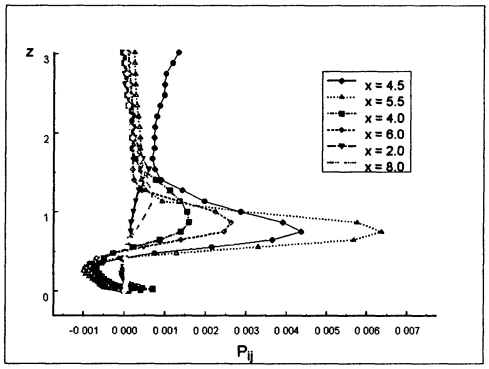

b)

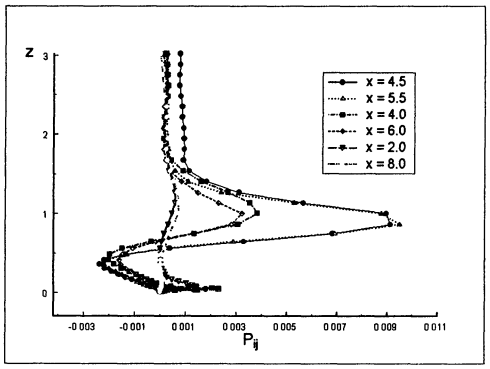

c)

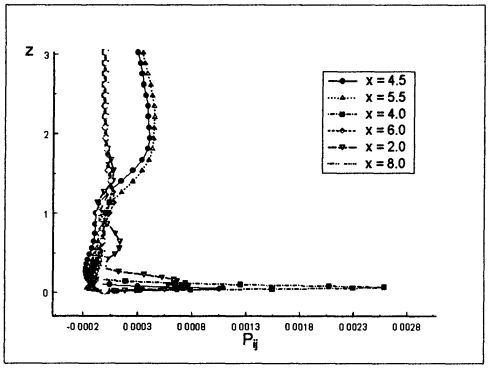

Fig. 4 Distribution of P_{ij} at different surface velcocity a)u_s = 0.5, b)1.0 and c) 2.0

a)

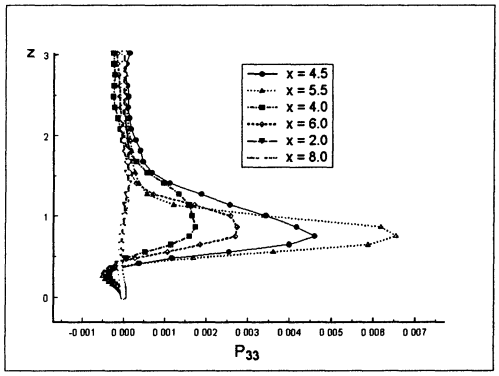

b)

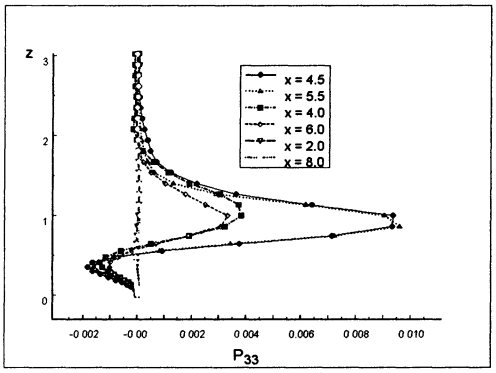

Fig. 5 Distribution of P_{33} for a) u_s = 0.5 and b) 1.0

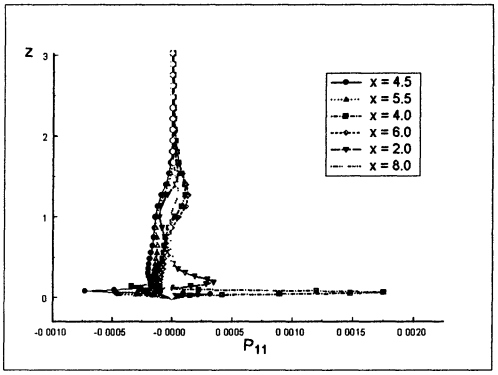

Fig. 6 Distribution of P_{11} for u_s = 2.0

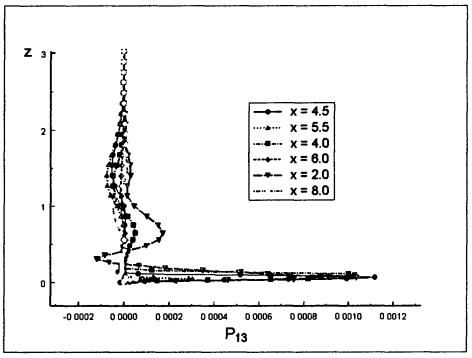

Fig. 7 Distribution of P_{13} for $u_s = 2.0$

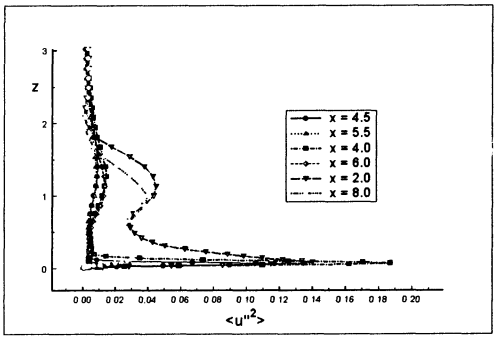

Fig. 10 Distribution of $\langle u''^2 \rangle$ for $u_s = 2.0$

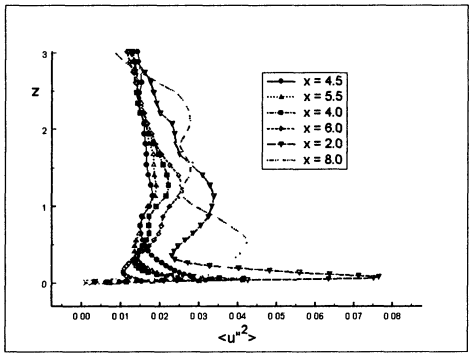

Fig. 8 Distribution of $\langle u''^2 \rangle$ for $u_s = 1.0$

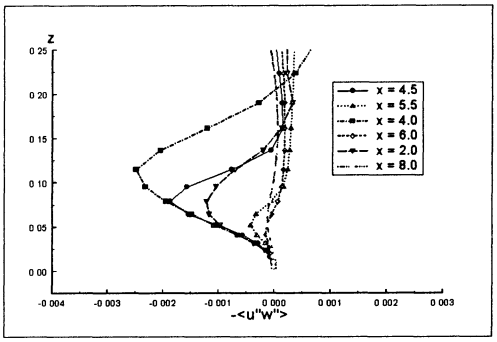

Fig. 11 Distribution of $\langle u'w' \rangle$ for $u_s = 2.0$

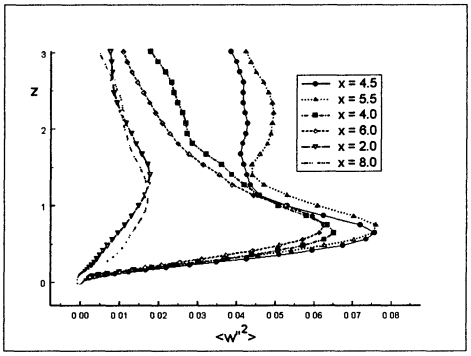

Fig. 9 Distribution of $\langle w''^2 \rangle$ for $u_s = 1.0$

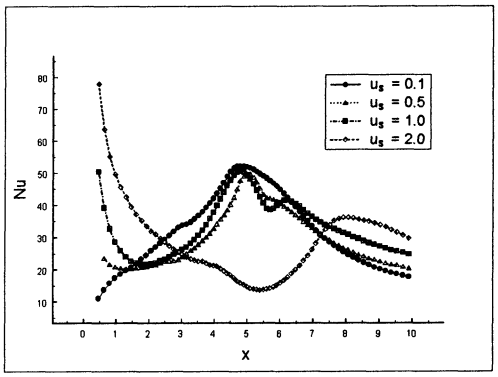

Fig. 12 Nusselt number distribution